nature physics

Article

https://doi.org/10.1038/s41567-024-02680-0

In-beam spectroscopy reveals competing nuclear shapes in the rare isotope ^{62}Cr

Received: 17 March 2024

Accepted: 24 September 2024

Published online: 18 October 2024

Check for updates

Alexandra Gade[1,2] ✉, Brenden Longfellow[3], Robert V. F. Janssens[4,5], Duc D. Dao[6], Frédéric Nowacki[6], Jeffrey A. Tostevin[7], Akaa D. Ayangeakaa[4,5], Marshall J. Basson[1,2], Christopher M. Campbell[8], Michael P. Carpenter[9], Joseph Chung-Jung[1,2], Heather L. Crawford[8], Benjamin P. Crider[10], Peter Farris[1,2], Stephen Gillespie[1], Ava M. Hill[1,2], Silvia M. Lenzi[11], Shumpei Noji[1], Jorge Pereira[1], Carlotta Porzio[8], Alfredo Poves[12], Elizabeth Rubino[1] & Dirk Weisshaar[1]

In recent decades, rare-isotope facilities have enabled the study of short-lived, neutron-rich nuclei. Their measured properties indicate that shell structure changes in the regime of unbalanced neutron-to-proton ratios compared with that of stable nuclei. In the so-called islands of inversion in the nuclear chart—around the neutron-rich nuclei ^{32}Mg, ^{42}Si and ^{64}Cr, for example—the textbook shell model predicts spherical shapes due to the respective magic neutron numbers of 20, 28 and 40 of these nuclei. However, nuclei in these regions turn out to be deformed in their ground states. Another hallmark of these islands is shape coexistence, where a nucleus assumes different shapes with excitation energy. Here we present evidence for this phenomenon from the observation of an excited 0^+ state in ^{62}Cr, two neutrons away from the heart of the island of inversion around neutron number $N = 40$. We use large-scale shell-model calculations to interpret the results, and we report extrapolations for the doubly magic nucleus ^{60}Ca.

Just like in atomic physics, the shell model has been exceptionally successful for nuclei, even though they are composed of two constituents, protons and neutrons, that interact strongly and at short range. On the nuclear chart and near stability, nuclei with magic numbers of protons or neutrons are spherical in shape and more inert than their open-shell neighbours. As a result, they often serve as immutable cores in attempts to solve the nuclear many-body problem by restricting computations to a valence configuration space. Towards the fringes of the nuclear chart, nuclei, or rare isotopes, are short-lived and undergo a sequence of radioactive decays until reaching stability. In the past decades, rare-isotope facilities have enabled the study of short-lived, neutron-rich nuclei. Their measured properties indicate that the shell structure that is well established at stability changes substantially in the regime of unbalanced neutron-to-proton ratios. Energy gaps between shells that would normally correspond to magic numbers disappear and new shell gaps emerge[1–4]. There are several regions on the nuclear chart where such a breakdown of neutron magic numbers (N) occurs: around ^{12}Be, ^{32}Mg, ^{42}Si and ^{64}Cr with $N = 8$, 20, 28 and 40 (refs. 1,2),

[1]Facility for Rare Isotope Beams, Michigan State University, East Lansing, MI, USA. [2]Department of Physics and Astronomy, Michigan State University, East Lansing, MI, USA. [3]Lawrence Livermore National Laboratory, Livermore, CA, USA. [4]Department of Physics and Astronomy, University of North Carolina at Chapel Hill, Chapel Hill, NC, USA. [5]Triangle Universities Nuclear Laboratory, Duke University, Durham, NC, USA. [6]Université de Strasbourg, CNRS, IPHC UMR7178, Strasbourg, France. [7]Department of Physics, Faculty of Engineering and Physical Sciences, University of Surrey, Guildford, UK. [8]Nuclear Science Division, Lawrence Berkeley National Laboratory, Berkeley, CA, USA. [9]Physics Division, Argonne National Laboratory, Argonne, IL, USA. [10]Department of Physics and Astronomy, Mississippi State University, Mississippi State, MS, USA. [11]Dipartimento di Fisica e Astronomia, Università degli Studi di Padova and INFN Sezione di Padova, Padua, Italy. [12]Departamento de Física Teórica and IFT-UAM/CSIC, Universidad Autónoma de Madrid, Madrid, Spain. ✉e-mail: gade@frib.msu.edu

https://doi.org/10.1038/s41567-024-02680-0

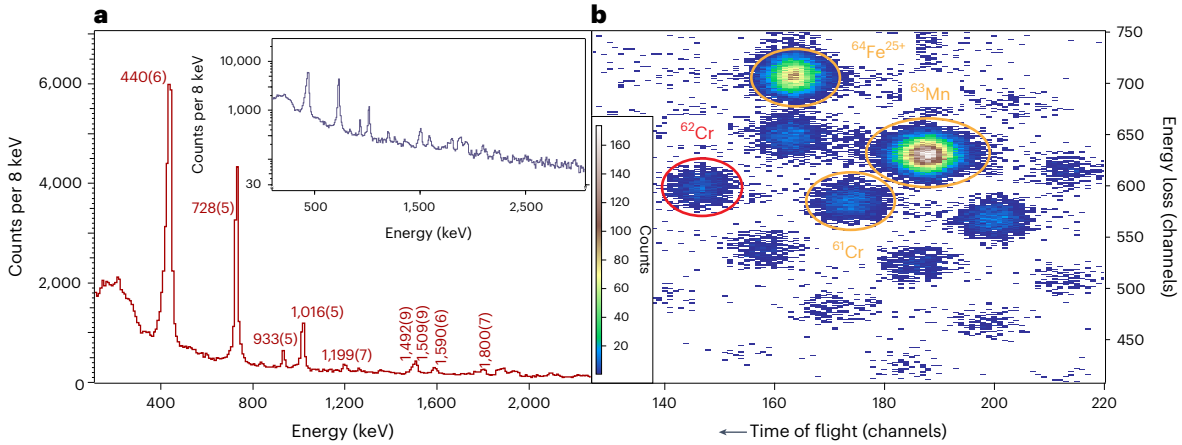

Fig. 1 | γ-ray and particle-identification spectra for ^{62}Cr. a, Event-by-event Doppler-reconstructed γ-ray spectrum of ^{62}Cr populated by two-proton removal from ^{64}Fe. The bins of the histogram cover 8 keV in energy. The visible peaks are labelled by their energies with uncertainties attributed to the determination of the peak position and the Doppler reconstruction. Inset: spectrum in logarithmic scale. There are many γ-ray transitions above 2,000 keV. **b**, Event-by-event particle identification through energy loss versus time of flight of the reaction residues entering the S800 spectrograph focal plane with ^{62}Cr (indicated in red) cleanly separated. For orientation, ^{61}Cr, ^{63}Mn and the 25$^+$ charge state of ^{64}Fe are labelled in orange. All particles shown in the spectrum have a γ-ray detection associated with them.

respectively. At stability, $N = 40$ is a subshell gap that was originally thought to stabilize doubly magic ^{68}Ni ($Z = 28, N = 40$), just four protons north from ^{64}Cr on the nuclear chart. These regions of marked change on the nuclear landscape are often referred to as islands of inversion because deformed, shell-breaking configurations are energetically favoured over closed-shell ones. In fact, the properties of these nuclei identify them as being among the most collective and deformed in their regions, and they display none of the properties associated with closed shells. Although often reported at the northern shores of islands of inversion[5–8], shape coexistence, which is the occurrence of 0$^+$ states associated with different shapes within a small excitation-energy window near the ground state, has remained elusive. At the heart of the islands, clear evidence for shape-coexisting 0$^+$ states has been reported only in ^{12}Be (ref. 9), ^{30,32}Mg (refs. 10,11) and ^{44}S (ref. 12) following experimental tours de force, but not in the $N = 40$ island of inversion.

From an experiment motivated by the shell-model prediction of a stunning case of shape coexistence in ^{62}Cr, we report here direct evidence for a low-lying 0$^+$ excited state in this nucleus, just two neutrons away from the heart of the $N = 40$ island of inversion. This result was found in an in-beam γ-ray spectroscopy measurement performed at the newly operational Facility for Rare Isotope Beams (FRIB) at Michigan State University. The sensitivity of the two-proton knockout ^{9}Be (^{64}Fe, ^{62}Cr + γ)X reaction to the final-state total angular momentum J of the residue[13–16], combined with spectroscopy using the Gamma-Ray Energy Tracking In-beam Nuclear Array (GRETINA), a γ-ray tracking array[17,18], resulted in a detailed level scheme for ^{62}Cr at low excitation energy. The data have been verified with large-scale shell-model (LSSM) calculations and interpreted within the framework of the discrete non-orthogonal shell model (DNO-SM), which enables an analysis in terms of nuclear shapes[19]. The results highlight the importance of axial shape asymmetry (triaxiality) for the observed excited collective structures. This rare nuclear shape is not typically connected to islands of inversion.

The results reported here have broader implications. Only recently discovered[20], the $N = 40$ isotone ^{60}Ca plays a pivotal role on the nuclear chart, and competing predictions as to its deformed or doubly magic (spherical) nature can be found in the literature[21–25]. Based on our data, we provide the most informed prediction about its structure to date.

Experimental procedures

The ^{64}Fe projectiles were produced in-flight through fragmentation[26] of a primary beam of ^{70}Zn, accelerated in the FRIB linear accelerator to 173 MeV/u and impinging on a stationary 4.2-mm-thick ^{9}Be production target within FRIB's advanced rare-isotope separator[27]. A 1.8-mm-thick Al wedge was used in the pre-separator to purify ^{64}Fe to 52%, with ^{65}Co (35%) being the only other intense component in the incoming beam. Using momentum slits and compression optics, the rare-isotope beam, which had a momentum width of $\Delta p/p = 0.4\%$, was delivered to the 100 mg cm^{-2} thick ^{9}Be reaction target in front of the S800 spectrograph[28]. Reaction products were identified on an event-by-event basis in the spectrograph's focal plane. The particle-identification spectrum for ^{62}Cr produced from the incoming ^{64}Fe beam at a 100.4 MeV/u mid-target energy is provided in Fig. 1b. The inclusive cross section for two-proton removal from ^{64}Fe to ^{62}Cr was determined to be $\sigma_{inc} = 0.59(4)$ mb.

The high-resolution γ-ray detection system GRETINA[17], an array of 48 36-fold segmented high-purity germanium crystals assembled into modules of four crystals each, was used to measure the prompt γ-rays emitted by ^{62}Cr residues. An online pulse-shape analysis was performed for its detector signals to determine the spatial coordinates of the γ-ray interactions within GRETINA[17,18]. These interaction points, together with the trajectory vectors of the reaction products as reconstructed with the spectrograph, enabled the event-by-event Doppler correction of the γ-rays emitted by ^{62}Cr at $v/c = 0.423$. Figure 1a provides these spectra for ^{62}Cr with addback[18] included, a method that corrects for the scattering of γ-rays between neighbouring crystals.

The ^{62}Cr level scheme

Based on our previous low-statistical studies of ^{62}Cr (ref. 29), the decay of the first excited 0$^+$ state to the 2_1^+ level was expected to be observed around 900–1,000 keV, with the 1,016 keV transition of ^{62}Cr then proposed as a candidate for this $0_2^+ \rightarrow 2_1^+$ decay. With the high statistics afforded by FRIB, a detailed γγ coincidence and γ-ray multiplicity analysis becomes possible. This revealed a previously unobserved transition at 933 keV, which is the best candidate for the decay from the predicted excited 0_2^+ state and, furthermore, places the 1,016 keV transition as feeding the 4_1^+ rather than the 2_1^+ level. The most intense transitions in the spectrum are at 439, 728 and 1,016 keV, corresponding to the known decays of the 2_1^+ and 4_1^+ states and, as we will demonstrate here, from the 6_1^+ level, respectively. Figure 2 shows that the 933 keV γ-ray feeds the 2_1^+ level but not the 4_1^+ one and that it has a γ-ray multiplicity of not more than 2, consistent with the proposed $0_2^+ \rightarrow 2_1^+ \rightarrow 0_1^+$ cascade in the absence of appreciable discrete feeding. The 1,016 keV transition, on the other hand, is clearly demonstrated to

https://doi.org/10.1038/s41567-024-02680-0

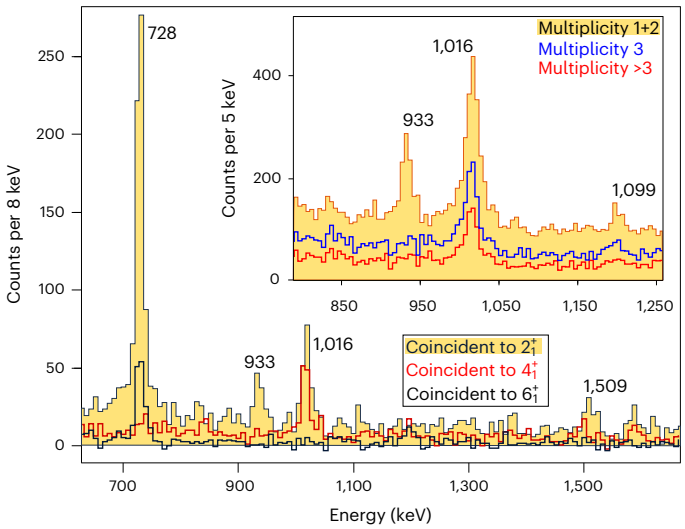

Fig. 2 | Spectra illustrating the γγ coincidence relationships for ^{62}Cr. The bins of the histograms cover 8 and 5 keV in energy, respectively. The peaks are labelled by their energy. Spectra coincident with the transitions of the 2_1^+, 4_1^+ and 6_1^+ levels, the strongest γ-rays in the spectrum of ^{62}Cr, are indicated in orange (filled), and by red and black lines, respectively. Inset: γ-ray multiplicity spectra, demonstrating that the 933 keV transition is part of a cascade of only 2 transitions (multiplicity 1 + 2, filled orange) whereas the neighbouring 1,016 keV transition has a multiplicity in excess of 3 (blue and red lines).

feed the 4_1^+ level with a γ-ray multiplicity of 3 and higher, consistent with a $6_1^+ \rightarrow 4_1^+ \rightarrow 2_1^+ \rightarrow 0_1^+$ sequence markedly fed from higher-lying states. A similar coincidence analysis was performed for all transitions reported here with the results summarized in Extended Data Table 1. The efficiency-corrected γ-ray intensities and the level scheme resulting from the coincidence relationships were used to determine the partial cross sections included in the table.

Characterization of the ^{62}Cr excited states

Two-proton (neutron) knockout from neutron (proton)-rich nuclei was shown to proceed as a direct reaction[30–33] where the shape of the longitudinal momentum distributions of the knockout residues, $p_\parallel$, encodes the total angular momentum[13,14] as well as the total orbital angular momentum[15,16] of the removed nucleons. When two-nucleon knockout occurs from a 0^+ ground state, an analysis of the final-state exclusive $p_\parallel$ distribution of the residue directly revealed the total angular momentum of this state, J. Final-state exclusive momentum distributions were obtained through software cuts of the γ-ray spectra applied to the inclusive longitudinal momentum distribution, including background and feeder subtraction, when possible. The results are displayed in Fig. 3 for the three states for which such an analysis was possible in terms of statistics, peak-to-background ratio in the γ-ray spectrum and predominance of feeding. For the 2_1^+ level, the first excited state, for example, a large number of suspected unobserved feeders prevented such an analysis. Figure 3 also presents the calculated momentum distributions, based on the reaction dynamics and formalism of ref. 15, using two-nucleon amplitudes from LSSM calculations using the Lenzi–Nowacki–Poves–Sieja (LNPS) interaction[21]. The calculated distributions were boosted into the laboratory frame and folded with the experimental resolutions. They are superimposed on the measured ones in Fig. 3 and support the J assignments (0^+) for the 1,379 keV level depopulated by a 933 keV γ-ray (Fig. 3b), 4_1^+ for the state at 1,174 keV decaying through a 728 keV line (Fig. 3c) and 6^+ for the 2,191 keV state de-excited through the 1,016 keV transition (Fig. 3d). As seen in Fig. 3a, the calculated 0_2^+ and 2_2^+ distributions are very similar in shape and, after folding in the experimental resolutions, overlap for all practical purposes. The assignment of the level, de-excited through the 933 keV transition as the 0_2^+ rather than the 2_2^+ state, is discussed below based on comparisons with the LSSM calculations.

The low-lying ^{62}Cr level scheme extracted from the present measurement is compared with LNPS shell-model calculations in Fig. 4b. The latter indicates that for each firmly placed level below 2.3 MeV, its shell-model counterpart was calculated within less than 100 keV, showing notable agreement between experiment and theory. The figure also includes the 1,509 keV γ-ray that is proposed to correspond to the $2_2^+ \rightarrow 2_1^+$ transition. It forms an energy doublet with a peak at 1,492 keV feeding the 4_1^+ state (inset of Fig. 4a). Obviously, no momentum distribution analysis was possible to confirm the 2_2^+ assignment. Similarly, a candidate for the third 2^+ level is proposed, for which the decays to the ground and 2_1^+ states are reported with a branching ratio close to the prediction. The notable good agreement with the shell-model calculations strongly supports the 0_2^+ assignment for the 1,379 keV state reported here as well as the 2_2^+ and 2_3^+ assignments. Note that, although both the 2_2^+ and the 2_3^+ levels are expected to decay to the 0_2^+ state, the predicted branching ratios for these transitions are too small to be observed in the present experiment. For example, the γ-ray corresponding to the $2_3^+ \rightarrow 0_2^+$ transition would have a peak area of less than 16% that of the 933 keV one (see the level scheme in Fig. 4b for the branching ratios).

From the longitudinal-momentum-distribution analysis, together with the successful comparison of the proposed level scheme to shell-model calculations, these data establish the 2_1^+, 4_1^+, 6_1^+, 0_2^+, 2_2^+ and 2_3^+ states in ^{62}Cr, a nucleus close to ^{64}Cr, the centre of the $N = 40$ island of inversion. In the following, we will discuss the structure and shape

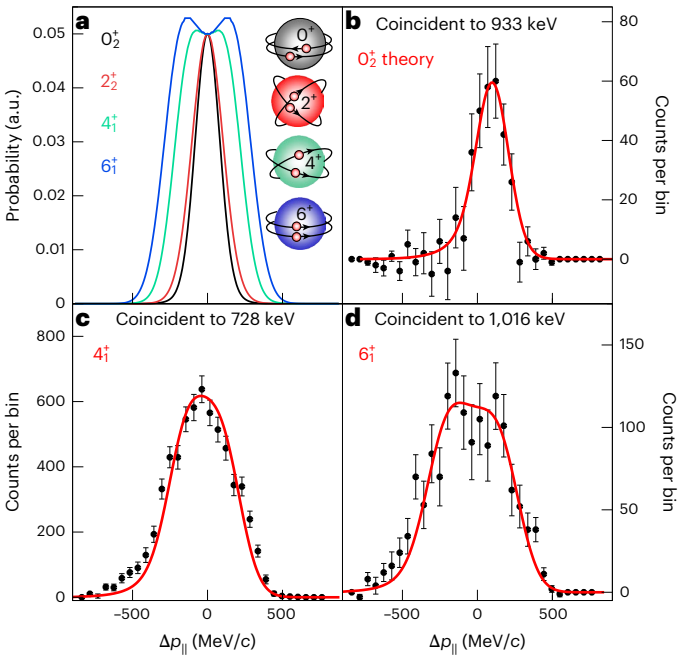

Fig. 3 | Measured and calculated longitudinal momentum distributions for ^{62}Cr. a–**d**, For the two-proton knockout to individual final states in ^{62}Cr, the shape of the longitudinal momentum distributions depends on the total angular momentum of the final state J, with the width increasing with J. **a**, The bare calculated momentum distributions transformed into the laboratory frame together with schematic configurations of the two protons that were knocked out in the reaction. **b**–**d**, Experimental data (black) compared with the calculated momentum distributions (red curves), folded with all experimental resolutions (Methods) and coincident to 933 keV (**b**), 728 keV (**c**) and 1,016 keV (**d**). Here, $\Delta p_\parallel = p_\parallel - p_0$, where $p_0 = 27.1$ GeV/c is the longitudinal momentum corresponding to a central path through the spectrometer and $p_\parallel$ is the event-by-event reconstructed longitudinal momentum of ^{62}Cr. The error bars are the statistical standard deviations as propagated through the subtractions. The bins of the histograms cover 53.4 MeV/c in momentum.

https://doi.org/10.1038/s41567-024-02680-0

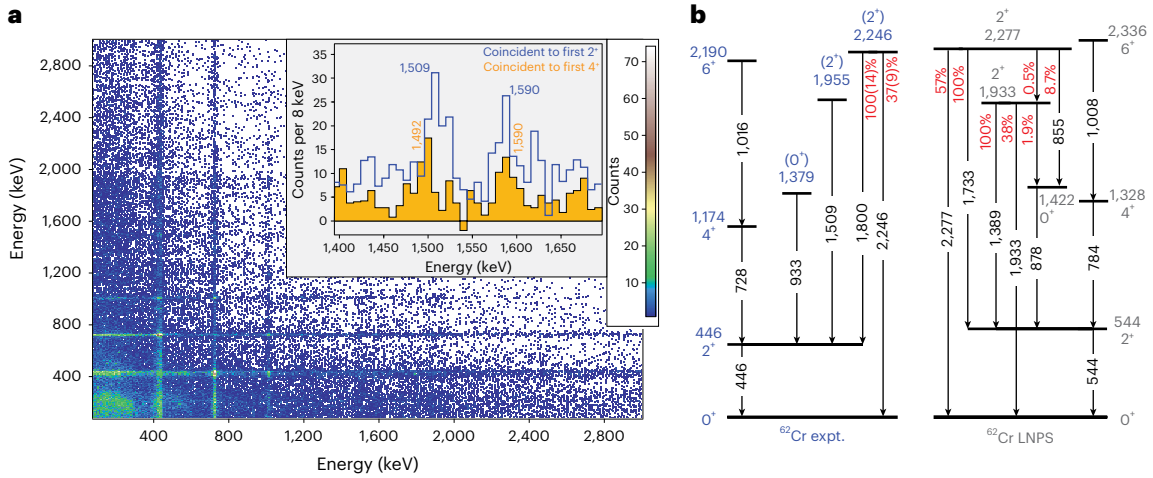

Fig. 4 | Experimental data underlying the level scheme of ^{62}Cr. a, γγ coincidence matrix and cuts of spectra in coincidence with 2_1^+ (blue) and 4_1^+ (orange, filled) states showing that the peak structure at 1,500 keV is a doublet. The 1,509 keV line is attributed to the $2_2^+ \rightarrow 2_1^+$ transition in coincidence with the 2_1^+ level. The relevant peaks are labelled by their energy. **b**, Comparison of the proposed (expt., experimental) low-lying level scheme (left) with the LNPS shell-model calculations discussed in the text (right). Shown are level energies and the associated J^π spins and parity (blue and grey for experiment and calculations, respectively) and γ-ray transition energies in black. Measured and calculated branching ratios are in red. J^π assignments in brackets are tentative.

of this key nucleus and present an informed prediction for the structure of the pivotal[20,22–25] $N = 40$ isotone ^{60}Ca.

Calculations and evidence of shape coexistence

In this section, the present experimental data are discussed in the context of LSSM diagonalizations and interpreted within the recently developed DNO-SM[19], which provides a description in terms of nuclear shapes. In both cases, the valence space is composed of the *pf* shell for protons and the $1p_{3/2}$, $0f_{5/2}$, $1p_{1/2}$, $0g_{9/2}$ and $1d_{5/2}$ orbitals for neutrons, on top of an inert ^{48}Ca core.

The interaction is the well-known LNPS Hamiltonian[21] with minor adjustments, which has enabled the successful description of many recent experimental findings in the neutron-rich region of the nuclear chart between ^{48}Ca and ^{78}Ni (refs. 29,34). As previously described, Fig. 4b compares the experimental and calculated level sequences; the agreement is excellent.

To characterize the spectroscopic shell-model results with respect to deformation and shapes, an analysis based on the DNO-SM model was undertaken. This approach enabled diagonalization of the same LNPS effective Hamiltonian and use of the same valence space within a relevant basis of deformed Hartree–Fock (HF) states from a potential energy surface represented in the (β, γ) plane. Here, β is the quadrupole deformation parameter and γ measures possible deviations from axial symmetry ($\gamma = 0°$ and 60° for axial prolate and oblate shapes, respectively).

Spectroscopic results for both methods are displayed in Fig. 5. The calculated states can be grouped into three collective structures: the ground-state band and two sidebands, hereafter labelled the yrast, excited and γ bands. These three all exhibit collectivity with large intra-band quadrupole transition strengths. In a traditional rotational picture, where the K quantum number is the projection of the total angular momentum onto the symmetry axis, the bands built on the 0_1^+ and 0_2^+ states would be assigned as $K = 0$ bands whereas that based on the 2_3^+ level would correspond to $K = 2$. Inspection of the properties of the 2_2^+ and 2_3^+ states indicates small spectroscopic quadrupole moments as well as a sizeable quadrupole transition between them. This points to K mixing and is associated with a degree of triaxial deformation. These findings were confirmed, as the first three states of each band expand into the (β, γ) plane, as shown in Fig. 6. The leading amplitudes are illustrated by orange circles. The following points are noteworthy: (1) There is a notable similarity in the expansion of the members in each band. (2) All three bands expand towards non-axial shapes. (3) The deformation is the largest for the yrast band. (4) The expansions on top of the 0_2^+ and 2_3^+ states closely mirror each other, indicating a clear correspondence between their respective characters.

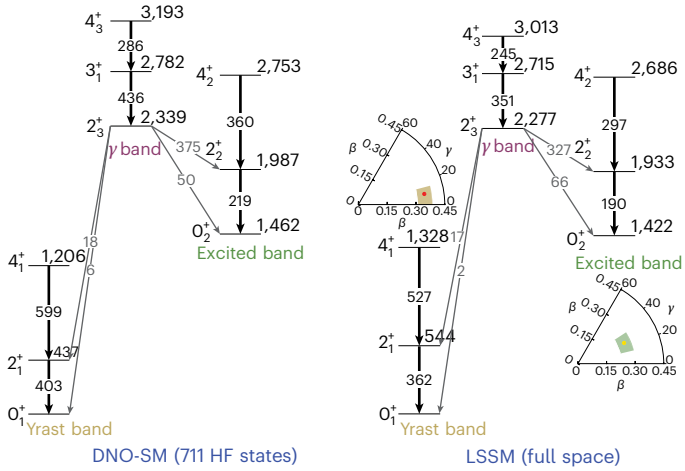

Fig. 5 | Level schemes predicted by the DNO-SM and LSSM calculations. The calculations used the same valence space and the LNPS effective interaction. The levels are labelled by excitation energy and J^π quantum numbers. Excited bands are predicted on top of the 2_3^+ and 0_2^+ states (labelled γ and excited band, respectively). Transitions within a band and out of the band structures are indicated by black and grey arrows, respectively, and are labelled by their transition strength. The Kumar invariants for the 0_1^+ and 0_2^+ states at fixed configurations (4p4h and 2p2h, respectively) are shown as well. The dots and shaded areas indicate the mean values of the β and γ deformations and their variances, respectively.

The nature of the collectivity in ^{62}Cr can be understood further from the quadrupole properties derived from the Nilsson-SU3 model[35]. An analysis following refs. 2,35, sketched in Extended Data Figs. 1 and 2 and Extended Data Table 2, revealed that the ^{62}Cr ground state can be characterized by four-particle, four-hole (4p4h) configurations associated with excitations across the $N = 40$ gap, which correspond to an axially symmetric solution. The excited bands, dominated by 2p2h configurations, correspond to a non-axially symmetric solution with K mixing. This is in agreement with the DNO expansion in Fig. 6, where the ground-state wavefunction is seen to develop around axial solutions ($\gamma \approx 0°$) and where both excited bands expand towards non-axial

https://doi.org/10.1038/s41567-024-02680-0

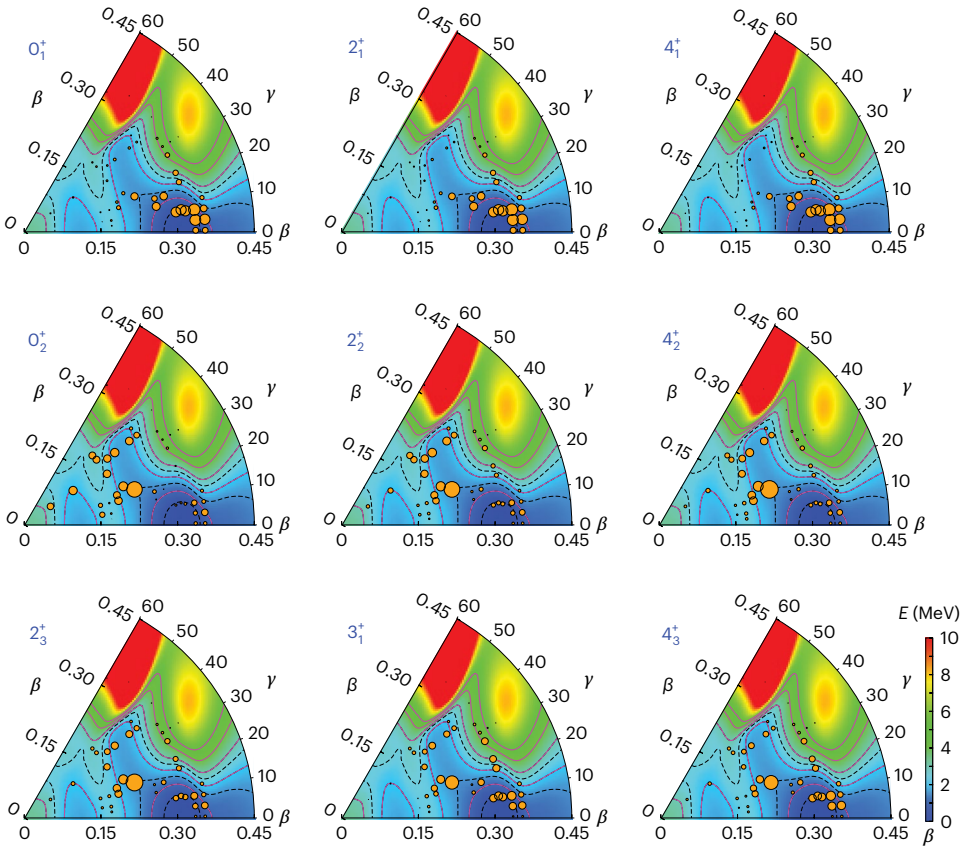

Fig. 6 | Potential energy surfaces in the β–γ deformation plane. For the states of ^{62}Cr labelled by J^π, the potential energy surface (potential energy E, colour-coded on a scale of mega-electronvolts with solid and dashed lines representing the energy contours with 1 and 0.5 MeV distance, respectively) reveals the importance of the triaxial degree of freedom ($\gamma = 30°$). The orange dots signal the dominant constrained HF configurations of the band structures. The area of an orange dot is directly proportional to the probability of the (β, γ) components in the total DNO wavefunction.

ones ($\gamma \approx 30°$). Based on these considerations, the three bands observed in ^{62}Cr can be viewed as remnants of pure 4p4h excitations for the yrast band and pure 2p2h configurations for the excited bands, the first being axially symmetric and the latter two triaxial. This is also consistent with the Kumar plots at fixed particle–hole content shown in Fig. 5.

Given the successful description of ^{62}Cr, we now extrapolate towards the neutron-rich end of the key calcium isotopic chain. Indeed, within the present theoretical description, the intruder features dominating the structure of ^{62}Cr extend to the titanium and calcium chains. Recent discussions of ^{60,62}Ti (refs. 23,36) indicated that there are quadrupole excitations with strong *npnh* content in the low-lying states. In the proton-magic calcium chain, the proton–neutron quadrupole force is no longer at play, but the neutron $N = 40$ shell gap is reduced (Fig. 28 in ref. 2), hence favouring pairing excitations from the *pf* to the *sdg* shells. The ^{56,58,60}Ca isotopes are predicted to exhibit constant 2^+ energies, as perhaps hinted at by recent measurements[24]. A large seniority $v = 0$ component was calculated for their ground states (meaning that there will be almost no unpaired neutrons), a signature of a superfluid regime[37]. A detailed decomposition of the ^{56,58,60}Ca ground-state wavefunctions is provided in Table 1.

As the energies of the first 2^+ states in neutron-rich even–even Ca nuclei were some of the telltale observables in early experiments that aimed to understand the evolution of nuclear structure towards ^{60}Ca, it is interesting to explore the consequences of the present calculations for these $E(2_1^+)$ values. The absolute 2^+ energies in these isotopes have all been predicted to lie between 1.5 and 2.0 MeV, which is slightly above experimental values when available[24]. A possible reason for this overestimation is the influence of the $s_{1/2}$ orbital computed to be at the Fermi surface in ^{60}Ca in ab initio coupled cluster calculations[38]. Preliminary calculations extending the valence space used here to incorporate this orbital for the calcium isotopes depopulate the $g_{9/2}$ and $d_{5/2}$ orbitals somewhat and, indeed, reduce the 2^+ excitation energies by about 300 keV, in agreement with recent experimental findings[24], pointing at another important factor in the description of the most neutron-rich Ca isotopes.

Table 1 | Characteristics of ^{56,58,60}Ca

Isotope	$n_{(g_9+d_5)}$	0p0h(%)	2p2h(%)	4p4h(%)	6p6h(%)	v=0(%)
^{56}Ca	1.3	46	44	9	0	98
^{58}Ca	2.2	21	50	26	3	95
^{60}Ca	3.4	5	35	46	13	90

Total occupation $n_{(g_9+d_5)}$ of the $g_{9/2}$ and $d_{5/2}$ neutron intruder orbitals and percentages for particle–hole excitations across the N=40 gap in the ground states of neutron-rich Ca isotopes. The last column is the seniority v=0 content in the ground-state wavefunction.

Outlook

Strong experimental and theoretical evidence has been provided for the observation of the excited 0_2^+, 2_2^+ and 2_3^+ states in ^{62}Cr, a central tenant of the $N = 40$ island of inversion. Within the framework of LSSM calculations complemented by DNO-SM computations, an interpretation in terms of nuclear shapes emerges in which the calculated shape-coexisting structure built on the 0_2^+ level is associated with a non-axial shape and is dominated by 2p2h intruder configurations straddling the $N = 40$ shell gap. This structure should be contrasted with the axially symmetric, strong prolate one calculated for the

collective band built on the ground state and predicted to be of dominant 4p4h character. The 4p4h components of the ground-state band then place ^{62}Cr as the portal to the $N = 40$ island-of-inversion regime. Furthermore, the observed decay pattern together with the correspondence with the calculations leads to the assignment of the 2_3^+ state as the head of the predicted γ band. The calculations indicate sizeable mixing with the 0_2^+ band structure and a similar shape for both excitations. Armed with this agreement between experiment and theory, we extrapolate towards the nominally doubly magic ^{60}Ca nucleus and predict a 2_1^+ excitation energy of the order of ~1 MeV as in the $N = 36$ and 38 isotones. Further tests of the detailed predictions for nuclear shapes and associated shell-model configurations in ^{62}Cr will soon be possible, for example, by using low-energy Coulomb excitation and comprehensive transfer reactions, as FRIB's capabilities are ramped up.

Online content

Any methods, additional references, Nature Portfolio reporting summaries, source data, extended data, supplementary information, acknowledgements, peer review information; details of author contributions and competing interests; and statements of data and code availability are available at https://doi.org/10.1038/s41567-024-02680-0.

References

1. Brown, B. A. The nuclear shell model towards the drip lines. *Physics* **4**, 525–547 (2022).
2. Nowacki, F., Obertelli, A. & Poves, A. The neutron-rich edge of the nuclear landscape: experiment and theory. *Prog. Part. Nucl. Phys.* **120**, 103866 (2021).
3. Otsuka, T., Gade, A., Sorlin, O., Suzuki, T. & Utsuno, Y. Evolution of shell structure in exotic nuclei. *Rev. Mod. Phys.* **92**, 015002 (2020).
4. Sorlin, O. & Porquet, M.-G. Nuclear magic numbers: new features far from stability. *Prog. Part. Nucl. Phys.* **61**, 602–673 (2008).
5. Rotaru, F. et al. Unveiling the intruder deformed 0_2^+ state in ^{34}Si. *Phys. Rev. Lett.* **109**, 092503 (2012).
6. Suchyta, S. et al. Shape coexistence in ^{68}Ni. *Phys. Rev. C* **89**, 021301 (2014).
7. Mărginean, N. et al. Shape coexistence at zero spin in ^{64}Ni driven by the monopole tensor interaction. *Phys. Rev. Lett.* **125**, 102502 (2020).
8. Gade, A. & Liddick, S. N. Shape coexistence in neutron-rich nuclei. *J. Phys. G: Nucl. Part. Phys.* **43**, 024001 (2016).
9. Shimoura, S. et al. Lifetime of the isomeric 0_2^+ state in ^{12}Be. *Phys. Lett. B* **654**, 87–91 (2007).
10. Schwerdtfeger, W. et al. Shape coexistence near neutron number $N=20$: first identification of the E0 decay from the deformed first excited $J^\pi=0^+$ state in ^{30}Mg. *Phys. Rev. Lett.* **103**, 012501 (2009).
11. Wimmer, K. et al. Discovery of the shape coexisting 0^+ state in ^{32}Mg by a two neutron transfer reaction. *Phys. Rev. Lett.* **105**, 252501 (2010).
12. Force, C. et al. Prolate-spherical shape coexistence at $N=28$ in ^{44}S. *Phys. Rev. Lett.* **105**, 102501 (2010).
13. Simpson, E. C., Tostevin, J. A., Bazin, D., Brown, B. A. & Gade, A. Two-nucleon knockout spectroscopy at the limits of nuclear stability. *Phys. Rev. Lett.* **102**, 132502 (2009).
14. Simpson, E. C., Tostevin, J. A., Bazin, D. & Gade, A. Longitudinal momentum distributions of the reaction residues following fast two-nucleon knockout reactions. *Phys. Rev. C* **79**, 064621 (2009).
15. Simpson, E. C. & Tostevin, J. A. Correlations probed in direct two-nucleon removal reactions. *Phys. Rev. C* **82**, 044616 (2010).
16. Longfellow, B. et al. Two-neutron knockout as a probe of the composition of states in ^{22}Mg, ^{23}Al, and ^{24}Si. *Phys. Rev. C* **101**, 031303 (2020).
17. Paschalis, S. et al. The performance of the gamma-ray energy tracking in-beam nuclear array GRETINA. *Nucl. Instrum. Methods Phys. Res. Sect. A* **709**, 44–55 (2013).
18. Weisshaar, D. et al. The performance of the γ-ray tracking array GRETINA for γ-ray spectroscopy with fast beams of rare isotopes. *Nucl. Instrum. Methods Phys. Res. Sect. A* **847**, 187–198 (2017).
19. Dao, D. D. & Nowacki, F. Nuclear structure within a discrete nonorthogonal shell model approach: new frontiers. *Phys. Rev. C* **105**, 054314 (2022).
20. Tarasov, O. B. et al. Discovery of ^{60}Ca and implications for the stability of ^{70}Ca. *Phys. Rev. Lett.* **121**, 022501 (2018).
21. Lenzi, S. M., Nowacki, F., Poves, A. & Sieja, K. Island of inversion around ^{64}Cr. *Phys. Rev. C* **82**, 054301 (2010).
22. Magilligan, A., Brown, B. A. & Stroberg, S. R. Data-driven configuration-interaction Hamiltonian extrapolation to ^{60}Ca. *Phys. Rev. C* **104**, L051302 (2021).
23. Gade, A. et al. Nuclear structure towards $N=40$ ^{60}Ca: in-beam γ-ray spectroscopy of ^{58,60}Ti. *Phys. Rev. Lett.* **112**, 112503 (2014).
24. Chen, S. et al. Level structures of ^{56,58}Ca cast doubt on a doubly magic ^{60}Ca. *Phys. Lett. B* **843**, 138025 (2023).
25. Li, J. Merging of the island of inversion at $N=40$ and $N=50$. *Phys. Lett. B* **840**, 137893 (2023).
26. Morrissey, D. J. & Sherrill, B. M. Radioactive nuclear beam facilities based on projectile fragmentation. *Philos. Trans. R. Soc. A* **356**, 1985–2006 (1998).
27. Portillo, M. et al. Commissioning of the advanced rare isotope separator ARIS at FRIB. *Nucl. Instrum. Methods Phys. Res. Sect. B* **540**, 151–157 (2023).
28. Bazin, D., Caggiano, J., Sherrill, B., Yurkon, J. & Zeller, A. The S800 spectrograph. *Nucl. Instrum. Methods Phys. Res. Sect. B* **204**, 629–633 (2003).
29. Gade, A. et al. In-beam γ-ray spectroscopy of ^{62,64}Cr. *Phys. Rev. C* **103**, 014314 (2021).
30. Bazin, D. et al. New direct reaction: two-proton knockout from neutron-rich nuclei. *Phys. Rev. Lett.* **91**, 012501 (2003).
31. Tostevin, J. A., Podolyák, G., Brown, B. A. & Hansen, P. G. Correlated two-nucleon stripping reactions. *Phys. Rev. C* **70**, 064602 (2004).
32. Tostevin, J. A. & Brown, B. A. Diffraction dissociation contributions to two-nucleon knockout reactions and the suppression of shell-model strength. *Phys. Rev. C* **74**, 064604 (2006).
33. Hansen, P. & Tostevin, J. Direct reactions with exotic nuclei. *Annu. Rev. Nucl. Part. Sci.* **53**, 219–261 (2003).
34. Rocchini, M. et al. First evidence of axial shape asymmetry and configuration coexistence in ^{74}Zn: suggestion for a northern extension of the $N=40$ island of inversion. *Phys. Rev. Lett.* **130**, 122502 (2023).
35. Zuker, A. P., Poves, A., Nowacki, F. & Lenzi, S. M. Nilsson-SU3 self-consistency in heavy $N=Z$ nuclei. *Phys. Rev. C* **92**, 024320 (2015).
36. Cortés, M. et al. Shell evolution of $N=40$ isotones towards ^{60}Ca: first spectroscopy of ^{62}Ti. *Phys. Lett. B* **800**, 135071 (2020).
37. Brink, D. & Broglia, R. *Nuclear Superfluidity* (Cambridge Univ. Press, 2005).
38. Hagen, G., Hjorth-Jensen, M., Jansen, G. R., Machleidt, R. & Papenbrock, T. Evolution of shell structure in neutron-rich calcium isotopes. *Phys. Rev. Lett.* **109**, 032502 (2012).

Methods

In-beam γ-ray spectroscopy

Exotic light and medium-mass nuclei furthest away from stability are efficiently produced by fragmentation of stable beams impinging upon stable targets at high beam energies. The resulting secondary rare-isotope beam, here ^{64}Fe, is then available for experiments at velocities in excess of $v/c = 0.4$. In the experimental scheme employed here, the excited states of the reaction residue, ^{62}Cr, produced in the collision of the fast rare-isotope beam with the target, were tagged through γ-ray spectroscopy, a technique that is subject to large Doppler shifts due to the high velocity of the emitter. The GRETINA γ-ray tracking array is highly segmented and enables subsegment position resolution from online signal decomposition[17,18]. The spatial coordinates x, y and z of the first interaction point of each γ-ray event within each germanium detector, as identified by the energy deposition being the largest, were then used to determine the γ-ray emission angle. The velocity of the emitting nucleus and the γ-ray emission angle were subsequently input into the event-by-event Doppler reconstruction, which transformed the γ-ray spectrum detected in the laboratory frame into the rest frame of the moving ^{62}Cr ion. As detailed in ref. 29, in-beam γ-ray spectroscopy at these high velocities bears an inherent energy uncertainty related to the precise target location relative to the GRETINA centre, the excited-state lifetime and whether the associated γ-ray emission point is within or behind the target. Such systematic errors are included in the uncertainties quoted for γ-ray transition energies in addition to the typically small fitting uncertainty and are why we used for the 2_1^+ excited-state energy the precise value from β decay rather than the value determined from the transition energy measured here.

Particle identification and reconstruction of momentum distributions in the S800 spectrograph

The projectile-like reaction residues emerging from the target were characterized event-by-event through their energy loss, measured in the S800 spectrograph's ionization chamber[28], their (x, y) positions and angles determined from two cathode read-out drift chambers, and time-of-flight measurements made between plastic scintillators in the DB3 position of the FRIB's fragment separator[27], the S800 analysis line object location and the back of the S800 focal plane. The energy loss was used to separate the observed isotopic chains by Z. The position and angle information measured in the focal plane, together with an ion optical transfer map that accounts for aberrations to fifth order, were used to reconstruct the longitudinal momentum distributions and were input into a trajectory correction of the time of flight, which was used to separate the masses A for a given isotopic chain with proton number Z. The S800 analysis beamline was operated in the so-called focus mode, where the beam was focused on the reaction target.

Reaction theory and comparisons of the measured and calculated parallel momentum distributions

A direct reaction model was used to predict the theoretical two-proton removal cross sections and the longitudinal momentum distributions of the residual ^{62}Cr nuclei[13–15]. The high incident velocities $v/c \approx 0.4$ enabled use of the eikonal approximation for the reaction dynamics[31–33], where the reacting constituents travel in straight-line paths for the short duration of their interactions. The protons were assumed to be removed in a single collision, as a result of elastic or inelastic interactions with a single ^{9}Be target nucleus. The interactions of the removed protons and residual nuclei with the target were described by complex optical potentials. The wavefunctions of the projectile (the incident ^{64}Fe projectile in its ground state) and of the populated final states of the residual nuclei (^{62}Cr(E^*, J^π)) were computed using LSSM. The details of the orbital occupancies of the correlated, removed protons (their two-nucleon amplitudes) were obtained from the overlaps, $\langle ^{62}\mathrm{Cr}\,(J^\pi)\,|\,^{64}\mathrm{Fe}\rangle$, of these many-body, shell-model wavefunctions. Combined, these physical inputs identified whether the two-proton removal reaction events arose from surface-grazing collisions of the projectile and target. The spectator core assumption implies that the proton-removing collisions did not alter the state of the nucleons making up the heavy residual nuclei. The differential removal cross sections, with respect to the longitudinal momenta of the ^{62}Cr residues, were calculated consistently within the same model[13–15].

The theoretical longitudinal-momentum distributions of the ^{62}Cr nuclei were calculated in the projectile rest frame and transformed into the laboratory frame, as seen in Fig. 3. They were then folded with a rectangular function to take into account the range of possible momentum losses through the thick ^{9}Be target by reactions occurring at different depths. Finally, the theoretical distributions were convolved with the experimental longitudinal-momentum distribution from unreacted ^{64}Fe projectiles (exploiting the charge state present in Fig. 1) in coincidence with γ-rays with energies above 500 keV. This approach empirically modelled the dissipative interactions taking place in the target and introduced the low-momentum tails ubiquitously observed in direct knockout[16,39]. The theoretical and experimental longitudinal-momentum distributions for different levels in ^{62}Cr are compared in Fig. 3. The theoretical values have been scaled and slightly shifted to best fit the central bins. The fitting results for each J^π hypothesis $\{0_2^+; 2_2^+; 4_1^+; 6_1^+\}$ are as follows: 933 keV with $\chi^2_{\mathrm{red}} = \{0.6; 1.0; 3.0; 4.3\}$, 728 keV with $\chi^2_{\mathrm{red}} = \{28.1; 16.4; 1.5; 3.1\}$ and 1,016 keV with $\chi^2_{\mathrm{red}} = \{9.8; 7.4; 1.9; 0.6\}$. The left tail, which was modelled only empirically, was omitted from the fit.

LSSM calculations

The LSSM calculations were performed within a valence space including the full *pf* shell for the protons and the $1p_{3/2}$, $0f_{5/2}$ and $1p_{1/2}$ orbitals together with the $\Delta j = 2$, $\Delta l = 2$, quasi-SU3 sequence $0g_{9/2}$, $1d_{5/2}$ for the neutrons. The original LNPS effective interaction was used[21] with only minor modifications. Such calculations have provided full-space diagonalizations involving bases of more than one billion Slater determinants. In the calculation of the Kumar invariants, we followed the sum-rule method discussed recently in ref. 40 to obtain an exact extraction of quadrupole invariants and their variances. The seniority of the calcium isotopes was extracted with the *J*-coupled code NATHAN[41,42]. This shell-model code expands the wavefunction into basis states of good seniority numbers using the quasi-spin formalism[43].

Discrete non-orthogonal shell model

In addition to the LSSM diagonalization, the recently developed DNO-SM[19] was used with the same model space and effective Hamiltonian. This method enables the decomposition of the shell-model wavefunctions into different deformed HF configurations, which provides direct access to their respective contributions to the deformation and, hence, enables a quantitative analysis in terms of nuclear shapes in both the ground and excited states. It is important to keep in mind that, variationally, the absolute DNO-SM spectra represent an upper bound to the exact shell-model spectra and that DNO-SM wavefunctions should converge to exact shell-model solutions. In ref. 19, only the quadrupole degrees of freedom (β, γ) and, in some cases, cranking components were included. The results presented in this work were obtained within the recently extended DNO-SM[ph] framework, which also simultaneously takes into account deformed HF states and particle–hole excitations built on top of these. Each DNO-SM state is then a superposition of both the deformed HF states (visualized as single points in the potential energy surface of Fig. 6) and their particle–hole excitations (lying a priori outside the (β, γ) potential energy surface). The expansion of the DNO-SM[ph] states was optimized in a two-step procedure. First, relevant deformed HF states in the (β, γ) plane were selected with the Caurier minimization technique developed in ref. 19, which allowed us to include the fewest constrained HF configurations without having to perform a full discretization of the entire potential energy surface. Next, particle–hole excitations on top of

the constrained HF states found in the first step were incorporated in the same manner. The DNO-SM results in Fig. 5 indicate an almost perfect match with the shell-model spectrum for all three bands. For instance, in general, the ground-state band would be more compressed (if confined to the quadrupole degrees of freedom only), due mostly to the lack of ground-state pairing correlations. A study of this extended DNO-SM[ph] approach will be presented elsewhere.

Algebraic SU3 analysis

The interpretation of collectivity can be supplemented by algebraic models. SU3 symmetry[44] assumes a valence space composed of a main harmonic oscillator shell with degenerate orbits with a pure quadrupole interaction. Under these assumptions, the nuclear configuration maximizing the quadrupole moment becomes the ground state. In mid-mass nuclei, the spin–orbit interaction breaks the degeneracy of the orbits and destroys the SU3 symmetry. Nevertheless, its variants—pseudo-SU3[45] and quasi-SU3[46]—can be applied in reduced shell-model spaces[35]. The pseudo-SU3 dynamical symmetry is achieved in an harmonic oscillator shell when the lowest large j shell is closed. For quasi-SU3 dynamical symmetry, this is the case when $\Delta j = 2$ orbits are present at the Fermi surface. In the present case, the LNPS valence space can be split into three groups of orbitals. For neutrons, the pseudo-SU3 symmetry applies in the space spanned by the $2p_{3/2}$, $2p_{1/2}$ and $1f_{5/2}$ orbitals, and the quasi-SU3 symmetry applies in the space formed by the $1g_{9/2}$, $2d_{5/2}$ and $3s_{1/2}$ orbitals. For protons, the quasi-SU3 symmetry applies in the space formed by the $1f_{7/2}$ and $2p_{3/2}$ orbits. The single-particle quadrupole moments were obtained by diagonalizing the quadrupole force in the LNPS space. Normalized quadrupole moments, Q_0/b^2, with b being the harmonic oscillator size parameter, are plotted in Extended Data Figs. 1 and 2 for different types of configuration.

The quadrupole moment of the nucleus was obtained by summing the single-particle moments. For ^{62}Cr, the maximum quadrupole moment, built from the four protons and ten neutrons above the ^{48}Ca core, was obtained by filling the Nilsson-SU3 'orbits'. Extended Data Fig. 1 illustrates the 4p4h ground state corresponding to four neutron particles in the quasi-*sdg* orbitals, four neutron holes in the pseudo-*sd* ones and four proton particles in quasi-*pf* orbits. The 2p2h configuration corresponding to the excited band is given in Extended Data Fig. 2. From the obtained configurations, notice that the 4p4h configuration corresponds to an axial solution with a unique filling of the Nilsson-SU3 levels, whereas the 2p2h configuration corresponds to a non-unique filling of the Nilsson-SU3 levels for the neutron holes and, hence, results in K mixing and a triaxial shape.

Data availability

This submission includes as additional supplemental files the relevant data supporting the findings of these studies. Other data are available from the corresponding author upon reasonable request.

Code availability

The techniques developed and exploited in the unpublished computer codes used to generate the results reported in this paper are presented in detail in published works. These works and reasonable requests for clarifications of the techniques or computational methods used are available from the corresponding author.

References

39. Stroberg, S. R. et al. Single-particle structure of silicon isotopes approaching ^{42}Si. *Phys. Rev. C* **90**, 034301 (2014).
40. Poves, A., Nowacki, F. & Alhassid, Y. Limits on assigning a shape to a nucleus. *Phys. Rev. C* **101**, 054307 (2020).
41. Caurier, E., Martínez-Pinedo, G., Nowacki, F., Poves, A. & Zuker, A. P. The shell model as a unified view of nuclear structure. *Rev. Mod. Phys.* **77**, 427–488 (2005).
42. Caurier, E. & Nowacki, F. Present status of shell model techniques. *Acta Phys. Pol. B* **30**, 705–714 (1999).
43. Arima, A. & Ichimura, M. Quasi-spin formalism and matrix elements in the shell model. *Prog. Theor. Phys.* **36**, 296–312 (1966).
44. Elliott, J. P. Collective motion in the nuclear shell model. I. Classification schemes for states of mixed configurations. *Proc. R. Soc. Lond. A* **245**, 128–145 (1958).
45. Arima, A., Harvey, M. & Shimizu, K. Pseudo LS coupling and pseudo SU(3) coupling schemes. *Phys. Lett. B* **30**, 517–522 (1969).
46. Zuker, A. P., Retamosa, J., Poves, A. & Caurier, E. Spherical shell model description of rotational motion. *Phys. Rev. C* **52**, R1741–R1745 (1995).

Acknowledgements

This material is based upon work supported by the US Department of Energy (DOE), Office of Science, Office of Nuclear Physics and used resources of FRIB Operations, which is a DOE Office of Science User Facility (Award No. DE-SC0023633). Further support by the DOE, Office of Science, Office of Nuclear Physics was provided under Grant Nos. DE-FG02-97ER410541 and DE-SC0023010 (University of North Carolina), DE-FG02-94ER40848 (Triangle Universities Nuclear Laboratory) and DE-AC02-05CH11231 (Lawrence Berkeley National Laboratory) and under Contract DE-AC02-06CH11357 (Argonne National Laboratory) as well as by the Office of High Energy Physics (Grant No. DE-SC0022299, TRAIN-MI). Support was provided by the DOE National Nuclear Security Administration through the Nuclear Science and Security Consortium (Award No. DE-NA0003180). Work at Lawrence Livermore National Laboratory was performed under DOE Contract No. DE-AC52-07NA27344 and was supported by the Lab Directed Research and Development programme (Project No. 23-LW-047). B.P.C. acknowledges support from the National Science Foundation (Grant No. PHY-1848177, CAREER). J.A.T. acknowledges support from the Science and Technology Facilities Council, UK (Grant No. ST/V001108/1). A.P. is supported by Grant No. CEX2020-001007-S funded by MCIN/AEI/10.13039/501100011033 and PID2021-127890NB-I00 (Spain).

Author contributions

A.G., R.V.F.J. and J.A.T. conceived and led the proposal for the experiment based on discussions with and calculations from F.N., S.M.L. and A.P. C.M.C., S.G., S.N., J.P. and D.W. led the operations of the experimental instruments used. A.G., B.L., R.V.F.J., A.D.A., M.J.B., C.M.C., M.P.C., J.C.-J., H.L.C., B.P.C., P.F., A.M.H., C.P. and E.R. staffed the shifts and monitored the online data quality. A.G. and B.L. led the data analysis. A.G., B.L., R.V.F.J., D.D.D., F.N. and J.A.T. led the interpretation of the data and wrote the first draft. J.A.T., D.D.D., F.N. and A.P. performed the reaction theory and nuclear structure theory calculations.

Competing interests

The authors declare no competing interests.

Additional information

Extended data is available for this paper at https://doi.org/10.1038/s41567-024-02680-0.

Supplementary information The online version contains supplementary material available at https://doi.org/10.1038/s41567-024-02680-0.

Correspondence and requests for materials should be addressed to Alexandra Gade.

Peer review information *Nature Physics* thanks Anna Corsi, Calvin Johnson and the other, anonymous, reviewer(s) for their contribution to the peer review of this work.

https://doi.org/10.1038/s41567-024-02680-0

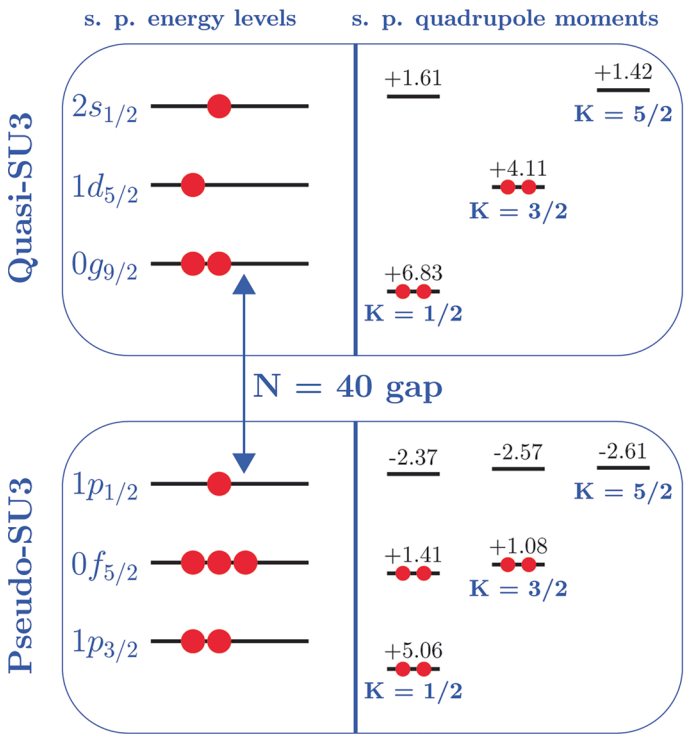

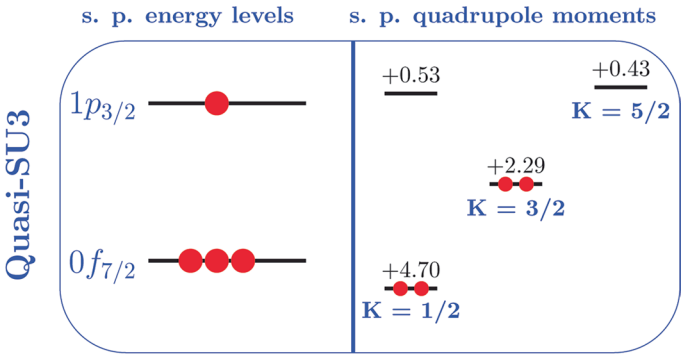

Extended Data Fig. 1 | Quasi- and Pseudo-SU3 plots for the 4p4h configuration in ^{62}Cr. Left: neutron valence space and single-particle quadrupole moments characterized by the projection of the total angular momentum on the symmetry axis, *K*. Right: same illustration for protons. The 4p4h configuration corresponds to an axial solution with unique filling of the Nilsson-SU3 levels. The red dots indicate the occupation of the single-particle orbitals with neutrons and protons, respectively.

https://doi.org/10.1038/s41567-024-02680-0

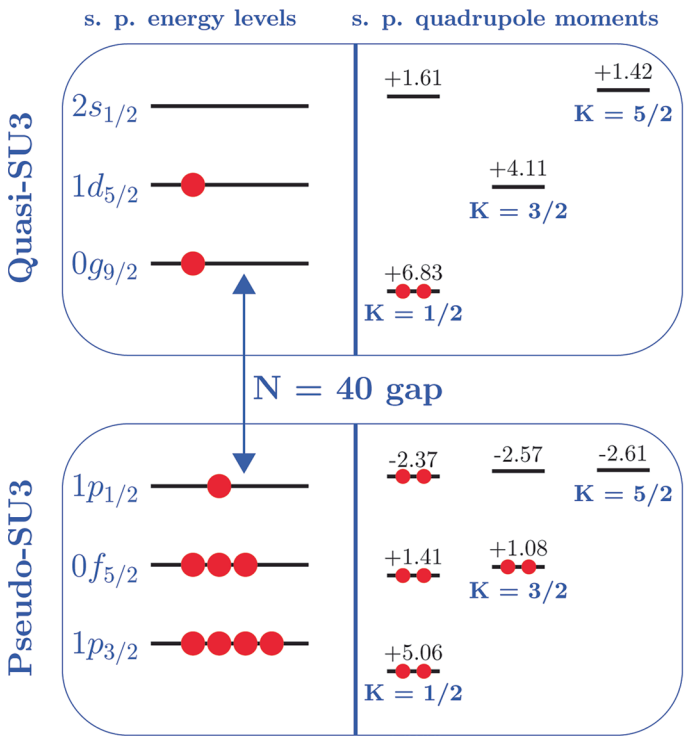

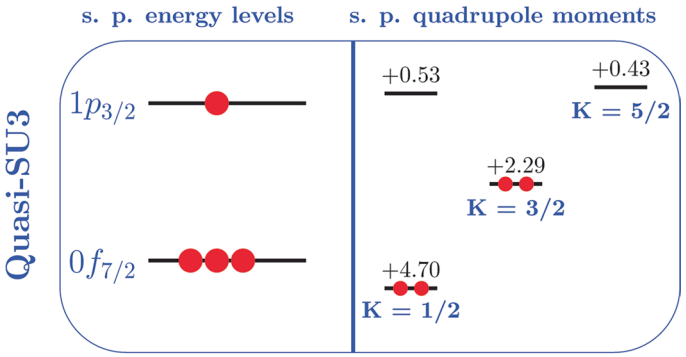

Extended Data Fig. 2 | Quasi- and Pseudo-SU3 plot for the 2p2h configuration in ^{62}Cr. Left: neutron valence space and single-particle quadrupole moments characterized by the projection of the total angular momentum on the symmetry axis, *K*. Right: same plot for protons. The 2p2h configuration corresponds to a non-unique Nilsson-SU3 levels filling for the neutron holes and, hence, *K* mixing and a triaxial shape. The red dots indicate the occupation of the single-particle orbitals with neutrons and protons, respectively.

https://doi.org/10.1038/s41567-024-02680-0

Extended Data Table 1 | States populated in ^{62}Cr in the two-proton removal from ^{64}Fe projectiles

E_J (keV)	J	σ_J^{exp} (mb)	σ_J^{th} (mb)	E_γ (keV)	E_f (keV)	J_f
0	0_1^+	0.114(5)	0.298			
446	2_1^+	0.14(1)	0.040	440(6)	0	0_1^+
1174	4_1^+	0.13(1)	0.037	728(5)	446	2_1^+
1379	(0_2^+)	0.019(2)	0.093	933(5)	446	2_1^+
1955	(2_2^+)	0.018(3)	0.047	1509(9)	446	2_1^+
2191	6_1^+	0.046(5)	0.022	1016(5)	1174	4_1^+
2246	(2_3^+)	0.023(3)	0.073	1800(7)	446	2_1^+
				2247(7)	0	0_1^+
2667		0.009(2)		1492(9)	1174	4_1^+
2764		0.015(2)		1590(6)	1174	4_1^+
3054		0.028(3)		1880(8)	1174	4_1^+
3390		0.010(2)		1199(7)	2191	6_1^+
4127		0.019(2)		1937(8)	2191	6_1^+
2011		0.003(1)		837(7)	1174	4_1^+
2437		0.004(1)		1262(7)	1174	4_1^+
2941		0.006(2)		1767(8)	1174	4_1^+

Listed are the excitation energy E_J and its spin-parity J, measured (exp) and calculated (th) cross sections σ, transition energy E_γ, final-state energy E_f and spin-parity J_f. Spin-parity assignments in brackets are based on comparison with theory. There are unplaced γ rays at 2095, 2125, 2213, and 2965 keV that, in total, carry 0.029 mb of cross section. States in italic are tentative – a coincidence of the corresponding transition with the 4_1^+ was firmly observed but, due to low statistics, the possibility that these transitions are actually feeding the 6^+ state cannot be excluded. The partial cross section to the ground state was obtained from the inclusive one via subtraction. In addition to the uncertainty originating from unplaced, observed potential feeders, the possibility of unobserved feeding will make all partial cross sections upper limits except for $\sigma(0_2^+)$ for which the absence of any significant feeding is argued via Fig. 2. The inclusive cross section is 0.59(4) mb.

https://doi.org/10.1038/s41567-024-02680-0

Extended Data Table 2 | Computed electric quadrupole transition strength, $B(E2; 2_1^+ \rightarrow 0_1^+)$, using different models

$B(E2;\ 2_1^+ \rightarrow 0_1^+)(e^2\mathrm{fm}^4)$						
$npnh$	QPSU3	PHF	n fix	DNO-SM	SM	exp
0p0h	153	120	117			
2p2h	308	290	279	403	365	325(44)
4p4h	445	468	452			

Results for Quasi/Pseudo-SU3 estimations (QPSU3), Projection of Hartree-Fock solutions (PHF) having the same particle-hole *npnh* configuration as the QPSU3 estimate, LSSM calculation using the fixed np-nh configurations (n fix), DNO shell-model calculations (DNO-SM), shell-model diagonalization (SM) for the case of ^{62}Cr, and the measured value (exp). Comparing the results from SM, DNO-SM, and n fix, one can see that the ground state is rather of 4p4h nature with a slight residual mixing in the wave function which reduces the SM B(E2) value with respect to the 'n fix' calculation.